

Quantifying non-Hermiticity using single- and many-particle quantum properties

Soumik Bandyopadhyay,^{1,2,*} Philipp Hauke,^{1,2,†} and Sudipto Singha Roy^{1,2,3,‡}

¹*Pitaevskii BEC Center, CNR-INO and Dipartimento di Fisica,
Università di Trento, Via Sommarive 14, Trento, I-38123, Italy*

²*INFN-TIFPA, Trento Institute for Fundamental Physics and Applications, Trento, Italy*

³*Department of Physics, Indian Institute of Technology (ISM) Dhanbad, IN-826004, Dhanbad, India*
(Dated: June 21, 2024)

The non-Hermitian paradigm of quantum systems displays salient features drastically different from Hermitian counterparts. In this work, we focus on one such aspect, the difference of evolving quantum ensembles under H_{nh} (right ensemble) versus its Hermitian conjugate, H_{nh}^\dagger (left ensemble). We propose a formalism that quantifies the (dis-)similarity of these right and left ensembles, for single- as well as many-particle quantum properties. Such a comparison gives us a scope to measure the extent to which non-Hermiticity gets translated from the Hamiltonian into physically observable properties. We test the formalism in two cases: First, we construct a non-Hermitian Hamiltonian using a set of imperfect Bell states, showing that the non-Hermiticity of the Hamiltonian does not automatically comply with the non-Hermiticity at the level of observables. Second, we study the interacting Hatano–Nelson model with asymmetric hopping as a paradigmatic quantum many-body Hamiltonian. Interestingly, we identify situations where the measures of non-Hermiticity computed for the Hamiltonian, for single-, and for many-particle quantum properties behave distinctly from each other. Thus, different notions of non-Hermiticity can become useful in different physical scenarios. Furthermore, we demonstrate that the measures can mark the model’s Parity–Time (PT) symmetry-breaking transition. Our findings can be instrumental in unveiling new exotic quantum phases of non-Hermitian quantum many-body systems as well as in preparing resourceful states for quantum technologies.

I. INTRODUCTION

The non-Hermitian paradigm of quantum systems, though often challenging our common understanding and interpretation of properties related to physical systems, may appear naturally as a result of valid physical processes. For instance, it may emerge via ubiquitous effects of noise in real quantum systems [1–3] or constrained dynamics realized via suppressing the quantum jumps in dissipative quantum dynamics [4–7]. In recent years, many concepts of Hermitian systems have been generalized to the non-Hermitian context, including bulk-boundary correspondence [8], topological characterization of non-Hermitian systems [9, 10], eigenstate thermalization [11, 12], many-body localization [13], etc. Moreover, apart from fundamental aspects, recent works also highlight promising applications of the non-Hermitian framework in the context of quantum technologies, such as in quantum thermal machines exploiting exceptional points [14] or enhanced quantum sensing [15–19]. Despite this importance, many fundamental aspects of non-Hermitian systems are still unclear. For instance, for a non-Hermitian system there exist different choices of eigenbasis (right, left, or mixed basis), which can yield results that lack a proper physical interpretation [20–22]. Even more, there is no clear framework how to quantify, using physically observable properties, the non-

Hermiticity of a given system.

Here, we present such a framework. To provide a concise overview, we briefly anticipate its main features, while we discuss its details in the bulk of the article. As is well known, the left and right eigenvectors diagonalizing a non-Hermitian Hamiltonian $H_{\text{nh}} = \sum_m \lambda_m |R_m\rangle\langle L_m|$, obeying $H_{\text{nh}}|R_m\rangle = \lambda_m|R_m\rangle$, $\langle L_m|H_{\text{nh}} = \langle L_m|\lambda_m$, and $\langle L_m|R_n\rangle = \delta_{mn}$, can in general be distinct, $\langle L_m| \neq (|R_m\rangle)^\dagger$. As we discuss, the evolution generated by H_{nh} leads an initial state to ensembles of right eigenvectors (including, e.g., single eigenstates reachable at large times), $\rho_{RR}(t) = \frac{e^{-itH_{\text{nh}}}\rho_{\text{in}}e^{itH_{\text{nh}}^\dagger}}{\text{Tr}[e^{-itH_{\text{nh}}}\rho_{\text{in}}e^{itH_{\text{nh}}^\dagger}]}$, such that observables measured on the system will physically be of the form $\langle R|\hat{O}|R\rangle$. In contrast, the evolution governed by H_{nh}^\dagger leads to ensembles of left eigenvectors, $\rho_{LL}(t) = \frac{e^{-itH_{\text{nh}}^\dagger}\rho_{\text{in}}e^{itH_{\text{nh}}}}{\text{Tr}[e^{-itH_{\text{nh}}^\dagger}\rho_{\text{in}}e^{itH_{\text{nh}}}]}$, and thus to expectation values of the form $\langle L|\hat{O}|L\rangle$. As we further show, the dynamics under *any* non-Hermitian Hamiltonian H_{nh} can be modeled as an effect of complete quantum measurements and subsequent post-selection of the results, giving a clear physical meaning to these expectation values in terms of observable properties. Unlike the Hermitian case, the evolution governed by H_{nh} and H_{nh}^\dagger may lead to results that can significantly differ from each other, due to a rich interplay between potentially complex λ_m and/or the difference between $\{|R_m\rangle\}$ and $\{\langle L_m|\}$. Our aim is to design measures that systematically capture these differences between H_{nh} and H_{nh}^\dagger , and thus quantify the non-Hermiticity of the system through observable properties.

As a first measure, we introduce the “Hamiltonian non-

* soumik.bandyopadhyay@unitn.it

† philipp.hauke@unitn.it

‡ sudipto@iitism.ac.in

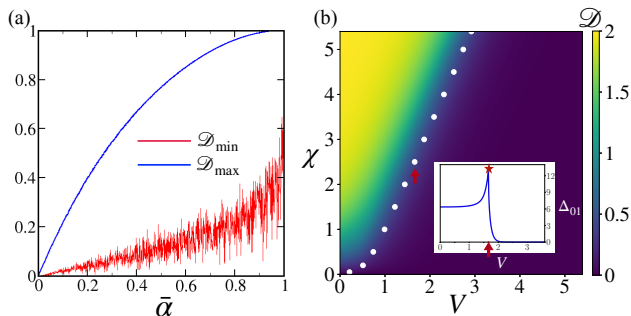


Figure 1. Behavior of degree of non-Hermiticity computed using $\mathcal{D} = \frac{\|H_{\text{nh}} - H_{\text{nh}}^\dagger\|}{\|H_{\text{nh}}\|}$ for two different non-Hermitian Hamiltonians. (a) Behavior of \mathcal{D} for $H_{\text{nh}}^{\text{Bell}}$ constructed using a set of imperfect Bell states as defined in Eqs. (16) and (17). For each value of the non-Hermiticity parameter $\bar{\alpha} = 1 - \alpha$, we plot the maximum (\mathcal{D}_{\max} , blue) and the minimum (\mathcal{D}_{\min} , red) within 1000 random realizations of the Hamiltonian obtained by choosing its energy eigenvalues $\{\lambda_m\}$ from a Gaussian distribution with zero mean and unit variance. While \mathcal{D}_{\min} increases only slowly and under strong fluctuations, \mathcal{D}_{\max} exhibits a clear monotonic growth with $\bar{\alpha}$. (b) Behavior of \mathcal{D} for the interacting non-Hermitian Hatano–Nelson model ($H_{\text{nh}}^{\text{HN}}$). At low values of interaction V , \mathcal{D} increases monotonically with asymmetric coupling χ and saturates to $\mathcal{D} \approx 2$. However, even for moderately large values of V , \mathcal{D} takes a significant non-zero value only beyond a threshold coupling, χ_c . Further, beyond $V \gtrsim 10^3$, \mathcal{D} remains zero for all values of χ considered in our analysis. In other words, under strong interactions the distance between $H_{\text{nh}}^{\text{HN}}$ and $(H_{\text{nh}}^{\text{HN}})^\dagger$ becomes insignificant in comparison to the norm of $H_{\text{nh}}^{\text{HN}}$ (see also Fig. 6 in Appendix C). The white circles correspond to the PT symmetry-breaking transition of the model marked by non-analytic behavior of the finite-size level-spacing $\Delta_{01} := \text{Re}(\lambda_1 - \lambda_0)$ (inset: Δ_{01} versus V for fixed $\chi = 2.5$). There is a striking agreement between the regions where \mathcal{D} drops and non-analyticities in Δ_{01} . The data is reported for $N = 12$ sites, half-filling, and with anti-periodic boundary conditions.

Hermiticity” $\mathcal{D} = \frac{\|H_{\text{nh}} - H_{\text{nh}}^\dagger\|}{\|H_{\text{nh}}\|}$, where $\|\cdot\|$ is the operator norm. This quantifier relies on knowledge of the full model Hamiltonian. In order to make non-Hermiticity more easily accessible, we further define the “non-Hermiticity score” as $SC_{\text{nh}}^{\mathcal{F}} = |\mathcal{F}_{RR}[\rho_{RR}] - \mathcal{F}_{LL}[\rho_{LL}]|$. This score quantifies the non-Hermiticity at the level of any physical state-dependent function $\mathcal{F}[\cdot]$ related to the model by measuring the difference when evaluating $\mathcal{F}[\cdot]$ for the state evolved under H_{nh} versus the one evolved under H_{nh}^\dagger .

The above formalism opens up the possibility to analyze to what extent the degree of non-Hermiticity of the Hamiltonian H_{nh} gets translated to the behavior of physically observable quantities. Moreover, we find situations where the Hamiltonian non-Hermiticity is small (due to a term with a large norm) while the non-Hermiticity score of simple observables is large, and vice

versa. Thus, different non-Hermiticity quantifiers complement each other, being able to reveal different notions of non-Hermiticity. Furthermore, as we demonstrate in our work, the scores may become instrumental in marking non-Hermitian phase transitions.

The rest of this article is organized as follows. In Sec. II, we introduce the formalism that provides an operational interpretation of dynamical evolution under any non-Hermitian Hamiltonian, unveil the physical meaning of the right and left eigenvectors associated with a non-Hermitian Hamiltonian, and introduce the quantifiers “Hamiltonian non-Hermiticity” as well as the “non-Hermiticity score.” In Sec. III, we illustrate the framework, first at the example of a non-Hermitian Hamiltonian constructed using a set of imperfect Bell states. Subsequently, we discuss the behavior in the interacting Hatano–Nelson model with asymmetric hopping, for which we compare non-Hermiticity of the model Hamiltonian and the non-Hermiticity score for single- as well as multi-site properties. Finally, in Sec. IV, we conclude with a brief discussion.

II. THEORETICAL BACKGROUND

In this section, we provide the theoretical framework for quantifying non-Hermiticity of a quantum system. We first discuss an operational interpretation of non-Hermitian dynamics as application of positive operator valued measurement on the system which is followed by a postselection. This interpretation shows that the resulting time-evolved state has a valid (albeit non-normalized) probability distribution, meaning observables can be measured and a physical meaning can be associated to them. Then, we show that the natural ensemble to evaluate expectation values is the ensemble of right and left eigenvectors for dynamics generated under H_{nh} and H_{nh}^\dagger , respectively. Finally, this naturally leads us to two (not necessarily equivalent) ways to quantify non-Hermiticity of a quantum system: through the difference between the matrices H_{nh} and H_{nh}^\dagger , and—perhaps more physically accessible—through the differences between expectation values reached by the evolution generated by H_{nh} and its hermitian conjugate.

A. Operational interpretation of dynamics under any non-Hermitian evolution

We start our discussion by providing an operational interpretation of dynamics governed by any generic non-Hermitian Hamiltonian H_{nh} . Let us consider a general quantum state

$$\rho(t) = \sum_{\lambda} p_{\lambda} \hat{P}_{\lambda}, \quad (1)$$

where \hat{P}_{λ} is a non-negative operator, $\hat{P}_{\lambda} = \hat{L}_{\lambda}^\dagger \hat{L}_{\lambda}$, and $p_{\lambda} \geq 0$ and $\sum_{\lambda} p_{\lambda} = 1$. Now, a dynamical evolution of

the above state under any map [23] would result in

$$\rho(t + \delta t) = \sum_m \mathcal{K}_m(\delta t) \rho(t) \mathcal{K}_m^\dagger(\delta t) = \sum_\lambda p_\lambda \hat{P}_\lambda, \quad (2)$$

where $\sum_m \mathcal{K}_m^\dagger \mathcal{K}_m = \mathbb{I}$ and $\hat{P}_\lambda = \sum_m \mathcal{K}_m(\delta t) L_\lambda^\dagger L_\lambda \mathcal{K}_m^\dagger(\delta t)$ is again a positive operator (because each summand $\mathcal{K}_m L_\lambda^\dagger L_\lambda \mathcal{K}_m^\dagger$ is), with $\hat{P}_\lambda \geq 0$ and $\sum_\lambda \hat{P}_\lambda = \mathbb{I}$.

We now consider a constrained evolution by projecting the evolved state $\rho(t + \delta t)$ onto a subspace,

$$\tilde{\rho}(t + \delta t) = \mathcal{P} \rho(t + \delta t) \mathcal{P} = \sum_\lambda p_\lambda \mathcal{M}_\lambda, \quad (3)$$

where $\mathcal{M}_\lambda = \mathcal{P} \hat{P}_\lambda \mathcal{P}$. In the case where $\mathcal{P} \neq \mathbb{I}$ (i.e., a projector onto a true subspace of the full Hilbert space), we have $\sum_\lambda \mathcal{M}_\lambda \neq \mathbb{I}$. The subspace restriction thus can lead to a loss of norm, $\text{Tr}(\tilde{\rho}(t + \delta t)) \leq 1$. Nevertheless, $\tilde{\rho}(t + \delta t)$ satisfies all the necessary conditions for a valid quantum state in the language of kinematic evolution:

(i) **Positive operator:** We have $\mathcal{M}_\lambda \geq 0$ and $p_\lambda \geq 0$. This implies $\tilde{\rho}(t + \delta t) \geq 0$.

(ii) **Positive measurement probabilities:** If we measure some quantum observable $\hat{O} = \sum_\ell a_\ell O_\ell$, the probabilities of distinct outcomes a_ℓ are positive, since using (i) we have $p_\ell \equiv \text{Tr}(O_\ell \tilde{\rho}(t + \delta t) O_\ell) \geq 0$.

Thus, while $\sum_\ell p_\ell = \text{Tr}(\tilde{\rho}(t + \delta t)) \leq 1$ is possible, probabilities of obtaining measurement results are always positive as expected from a physical observable. The remaining probability is associated to the cases where the system has leaked out into the subspace not considered (given by projector $\mathbb{I} - \mathcal{P}$). Hence, one can always assign an “operational meaning” or dynamical interpretation to any quantum state that satisfies the above two conditions. Before computing a quantity related to the system, it can be useful to normalize the quantum state $\tilde{\rho}(t + \delta t)$, as we do throughout this paper, so as to obtain the probabilities conditioned on the system being in the subspace, which sum up to identity.

We now show that the evolution under an arbitrary non-Hermitian Hamiltonian H_{nh} , defined on the system’s Hilbert space \mathcal{H}_S , can be written as a Kraus map acting on an extended space including an ancilla, $\mathcal{H}_S \otimes \mathcal{H}_A$, followed by a suitable projection. I.e., the evolution under any non-Hermitian Hamiltonian takes the form given by Eq. (3). The ancilla can be considered as any generic system ranging from qubits to bosonic baths. For the illustration purpose, here we consider it to be a qubit.

We start by constructing the evolution to leading order in a small time step δt , from which we obtain the continuous time evolution in the limit $\delta t \rightarrow 0$. Given any H_{nh} , one can always define the operators $\mathcal{K}_0 = (\mathbb{I}_S - iH_{\text{nh}}\delta t) \otimes \mathbb{I}_A$ and $\mathcal{K}_1 = \sqrt{\delta t(H_{\text{nh}}^\dagger - H_{\text{nh}})} \otimes \sigma_A^x$

acting in $\mathcal{H}_S \otimes \mathcal{H}_A$. Here, σ_A^x is the Pauli matrix and $\mathcal{K}_0^\dagger \mathcal{K}_0 + \mathcal{K}_1^\dagger \mathcal{K}_1 = \mathbb{I} + \mathcal{O}(\delta t^2)$. The dynamical evolution of an initial state operator $\rho(t)$ acting on $\mathcal{H}_S \otimes \mathcal{H}_A$ is given by

$$\rho(t + \delta t) = \mathcal{K}_0 \rho(t) \mathcal{K}_0^\dagger + \mathcal{K}_1 \rho(t) \mathcal{K}_1^\dagger. \quad (4)$$

This evolution describes a Master equation with jump operators \mathcal{K}_1 and is in the Kraus form as given in Eq. (2). (Note that the considered form of the operators \mathcal{K}_0 and \mathcal{K}_1 is not unique; in particular, a specific physical implementation yielding the same H_{nh} may be described microscopically by a different set of Kraus or unitary operators [24–29].)

To obtain the desired evolution, we assume the ancilla qubit to be initialized in the $|0\rangle\langle 0|$ state. We then employ dynamical evolution under the above map. Afterwards, we project the evolved state back onto $\mathcal{P}_0 = |0\rangle\langle 0|$. This amounts to using the qubit as a “flag” permitting post-selection onto the no-jump trajectory [5, 30]. The result is

$$\begin{aligned} \mathcal{P}_0 \rho(t + \delta t) \mathcal{P}_0 &= \mathcal{P}_0 \mathcal{K}_0 (\rho_S(t) \otimes |0\rangle\langle 0|) \mathcal{K}_0^\dagger \mathcal{P}_0 \\ &\quad + \mathcal{P}_0 \mathcal{K}_1 (\rho_S(t) \otimes |0\rangle\langle 0|) \mathcal{K}_1^\dagger \mathcal{P}_0 \\ &= (\mathbb{I}_S - iH_{\text{nh}}\delta t) \rho_S(t) (\mathbb{I}_S + iH_{\text{nh}}^\dagger \delta t) \otimes |0\rangle\langle 0| \\ &\quad + \mathcal{O}(\delta t^2). \end{aligned} \quad (5)$$

Therefore, in the limit of a small time step δt , the system undergoes the non-Hermitian evolution given by $e^{-itH_{\text{nh}}} \rho_S e^{itH_{\text{nh}}^\dagger}$, whereas the ancilla remains in the initialized $|0\rangle\langle 0|$ state. One can see this evolution as a quantum-Zeno effect, generated by the continuous monitoring described by \mathcal{P}_0 , and which freezes the ancilla to the $|0\rangle\langle 0|$ state. As is typical for the quantum-Zeno effect, the system undergoes a non-Hermitian evolution, describing the loss of norm out of the Zeno subspace [31–33].

In summary, if we consider a quantum system evolved under the effect of an *arbitrary* non-Hermitian system, we can always assign an operational meaning to the evolved states: they can be understood as *quantum states originated due to the action of a constrained dynamical evolution manifested using complete quantum measurement and postselection of the results*. This interpretation shows that the resulting time-evolved state has a valid probability distribution, meaning observables can be measured and a physical meaning can be associated to them.

B. Interpreting the eigenbasis of H_{nh}

As mentioned in the introduction, to compute physically relevant quantities of any non-Hermitian system, the non-unique choice of basis states often leads to anomalous behavior. In this section, we argue that expectation values evaluated in the right and left eigenvectors of the model have a valid physical origin [12, 34].

Let us consider a non-Hermitian Hamiltonian H_{nh} expressed in the biorthogonal basis

$$H_{\text{nh}} = \sum_m \lambda_m |R_m\rangle\langle L_m|, \quad (6)$$

where $\langle L_m|R_n\rangle = \delta_{mn}$ and the set of right (left) eigenvectors $\{|R_m\rangle\}$ ($\{\langle L_n|\}$) are not necessarily orthonormal. We now consider the evolution it generates,

$$\begin{aligned} \rho_{RR}(t) &= e^{-iH_{\text{nh}}t} \rho_{\text{in}} e^{itH_{\text{nh}}^\dagger}, \\ &= \sum_i e^{-i(\lambda_m - \lambda_n^*)t} a_{mn} |R_m\rangle\langle R_n|, \end{aligned} \quad (7)$$

where $a_{mn} = \langle L_m|\rho_{\text{in}}|L_n\rangle$. We can distinguish three situations.

1. All the λ_m 's have non-vanishing imaginary part with a non-degenerate $\max\{\Im[\lambda_{\tilde{m}}]\} = \lambda$.

Under this condition, Eq. (7) can be rewritten as

$$\begin{aligned} \rho_{RR}(t) &= \sum_m e^{2t\Im[\lambda_m]} a_{mm} |R_m\rangle\langle R_m| \\ &+ \sum_{m \neq n} e^{-it(\lambda_m - \lambda_n^*)} a_{mn} |R_m\rangle\langle R_n|. \end{aligned} \quad (8)$$

At large times, $\rho_{RR}(t)$ eventually converges to the right eigenvector with slowest decay rate [5, 34],

$$\rho_{RR}(t) \xrightarrow{t \rightarrow \infty} e^{2t\lambda} a_{\tilde{m}\tilde{m}} |R_{\tilde{m}}\rangle\langle R_{\tilde{m}}|. \quad (9)$$

In general, physical expectation values are given by $\text{Tr}(\rho_{RR}(t)\hat{O})$. Taking the trace in the biorthogonal basis that satisfies the completeness relation $\sum_m |R_m\rangle\langle L_m| = \mathbb{I}$, and using the relation $\langle R_n|L_k\rangle = \delta_{nk}$, we thus find physical observables will be obtained from the expectation values $\langle R_{\tilde{m}}|\hat{O}|R_{\tilde{m}}\rangle$.

2. All λ_m 's are real (Parity-Time symmetric case).

In this case, Eq. (7) reduces to

$$\begin{aligned} \rho_{RR}(t) &= \sum_m a_{mm} |R_m\rangle\langle R_m| \\ &+ a_{mn} \sum_{m \neq n} e^{-it(\lambda_m - \lambda_n)} |R_m\rangle\langle R_n|. \end{aligned} \quad (10)$$

This situation resembles the Hermitian case; neglecting resonances, the off-diagonal fluctuations are suppressed at large times, resulting in a diagonal ensemble consisting of the right eigenvectors given by

$$\rho_{RR}(t) \xrightarrow{t \rightarrow \infty} \sum_m a_{mm} |R_m\rangle\langle R_m|. \quad (11)$$

Similar to the previous case, here also the observables at long times are determined by (suitably weighted) matrix elements $\langle R_m|\hat{O}|R_m\rangle$ in the right eigenbasis.

3. Arbitrary non-Hermitian time evolution.

In the general scenario, an observable \hat{O} undergoes the evolution

$$\text{Tr}(\hat{O}\rho_{RR}(t)) = \sum_{mn} e^{-it(\lambda_m - \lambda_n^*)} a_{mn} \langle R_n|\hat{O}|R_m\rangle. \quad (12)$$

While the expression is more complicated, the matrix elements of the observable are still determined by the right eigenvectors, while the left eigenvectors enter through the overlap with the initial state via a_{mn} .

All the scenarios considered above illustrate the physical origin of expectation values evaluated in the right eigenvectors of the model. A similar analysis with H_{nh}^\dagger justifies the same reasoning for the left eigenvectors ($\{\langle L_m|\}$). As these considerations also show, while possibly containing interesting properties of the model [34], terms like $\langle R_m|\hat{O}|L_n\rangle$ do not naturally appear in the evaluation of physical quantities for the quantum state evolved under any generic non-Hermitian dynamics.

C. Non-Hermiticity quantifiers

The above considerations put us into the position to introduce two (nonequivalent) ways of quantifying non-Hermiticity through the full Hamiltonian or through observables.

1. Hamiltonian non-Hermiticity

As a first measure, we introduce the ‘‘Hamiltonian non-Hermiticity’’ (see also Fig. 1). It puts the qualitative notion of comparing a system Hamiltonian and its Hermitian conjugate onto quantitative grounds. We define it as

$$\mathcal{D} = \frac{\|H_{\text{nh}} - H_{\text{nh}}^\dagger\|}{\|H_{\text{nh}}\|}, \quad (13)$$

where $\|\cdot\|$ is the operator norm. This measure quantifies the distance between a model Hamiltonian H_{nh} and its Hermitian conjugate. It naturally vanishes for Hermitian systems. We find it most useful to normalize \mathcal{D} to the norm of H_{nh} , in order to avoid attributing significant non-Hermiticity to systems that are actually dominated by a large Hermitian part (see also Appendix C for a discussion about the unnormalized version). While it captures properties that the entire model system can in principle assume, quantifying non-Hermiticity via \mathcal{D} requires access to the full Hamiltonian matrix.

2. Non-Hermiticity score of observables

For practical purposes (in numerics or experiment), it may be of interest to construct quantifiers that—in contrast to \mathcal{D} —rely only on the use of observables. To this

end, we introduce the notion of “non-Hermiticity score” of an observable, defined as

$$SC_{\text{nh}}^{\mathcal{F}} = |\mathcal{F}_{RR}[\rho_{RR}] - \mathcal{F}_{LL}[\rho_{LL}]|. \quad (14)$$

This score quantifies the non-Hermiticity at the level of any computable physical quantity related to the model. It measures the difference of a state-dependent function $\mathcal{F}[\cdot]$ when evaluated for the state evolved under H_{nh} or under H_{nh}^\dagger , which as discussed above lead to ensembles of right or left eigenvectors ($\rho_{RR}(t)$ or $\rho_{LL}(t)$), respectively. As illustrated in the next section, one can choose for $\mathcal{F}[\cdot]$ single-body observables such as local magnetization or occupations as well as many-body observables such as von-Neumann entropy or purity. Following the discussions in Sec. II A, the corresponding expectation values are well-defined. The non-Hermiticity score thus expresses how much the non-Hermiticity of the model Hamiltonian is concretely translated into physical observables in a given time evolution.

Following also the discussion in Sec. II B, the density matrices ρ_{RR} and ρ_{LL} used to evaluate the score can represent the snapshot of a system at a given evolution time (see also Fig. 3 below) or they can correspond to individual eigenstates (Figs. 2). For the latter case, sometimes the non-Hermiticity score can depend significantly on the choice of eigenvectors. To have a state-independent analysis that captures the behavior across the spectrum, we can reformulate the non-Hermiticity score of Eq. (14) as a well-defined distance measure, given by

$$\|\overline{SC_{\text{nh}}^{\mathcal{F}}}\|_p = \left(\sum_{i=1} (SC_{\text{nh}}^{\mathcal{F}}[i])^p \right)^{\frac{1}{p}}. \quad (15)$$

This quantity is nothing but the p -norm of the vector $\overline{SC_{\text{nh}}^{\mathcal{F}}}$ with elements $\overline{SC_{\text{nh}}^{\mathcal{F}}} = \{SC_{\text{nh}}^{\mathcal{F}}[1], SC_{\text{nh}}^{\mathcal{F}}[2], \dots, SC_{\text{nh}}^{\mathcal{F}}[D]\}$, where $SC_{\text{nh}}^{\mathcal{F}}[k]$ denotes the non-Hermiticity score computed for the k -th eigenstate of the model, and D corresponds to the Hilbert space dimension. In our case, we will illustrate the results obtained for the case $p \rightarrow \infty$ (see Fig. 4), for which the above definition reduces to the infinity norm, $\|\overline{SC_{\text{nh}}^{\mathcal{F}}}\|_\infty = \max_i SC_{\text{nh}}^{\mathcal{F}}[i]$, which is the maximum value of the non-Hermiticity score computed over all the eigenstates of the model.

At the opposite limit, $p \rightarrow 0^+$, one obtains the 0-norm, which counts the number of eigenvectors with non-zero non-Hermiticity score and thus captures the qualitative behavior across the entire spectrum. In our analysis below, for convenience we use a numerical threshold $\mathcal{E}_{\text{Th}}^{\mathcal{F}}$, counting the total number of elements of $\overline{SC_{\text{nh}}^{\mathcal{F}}}$ with the condition $SC_{\text{nh}}^{\mathcal{F}}[k] \geq \mathcal{E}_{\text{Th}}^{\mathcal{F}}$. We denote the corresponding score by $\mathcal{G}^{\mathcal{F}}$. An example is plotted in Fig. 5.

III. ILLUSTRATION AT MODEL SYSTEMS

We are now equipped with ways to quantify the non-Hermiticity of a quantum system. In this section, we illus-

trate their behavior at two models. The first example has a quantum information-theoretic origin, namely, a non-Hermitian Hamiltonian constructed using a set of imperfect Bell states. In the second example, we consider a many-body Hamiltonian, the interacting Hatano–Nelson model, where non-Hermiticity is incorporated via asymmetric hopping between the sites. The findings related to both models highlight the inequivalency between different notions of non-Hermiticity.

A. Non-Hermitian model constructed using imperfect Bell state

In order to introduce the first example of the non-Hermitian Hamiltonian that we have considered in our work, we present a set of “imperfect” Bell states characterized by the parameter α ($0 < \alpha < 1$) and having the following mathematical form when expressed in the computational basis, given by

$$\begin{aligned} |R_{1,2}\rangle &= \frac{(\frac{1}{\alpha} - 1)|00\rangle + (|00\rangle \pm |11\rangle)}{\sqrt{1 + \frac{1}{\alpha^2}}}, \\ |R_{3,4}\rangle &= \frac{(1 - \alpha)|00\rangle + (|01\rangle \pm |10\rangle)}{\sqrt{(1 - \alpha)^2 + 2}}. \end{aligned} \quad (16)$$

For $\alpha = 1$, the above set of states reduces to the perfect set of Bell states, $|\Psi^\pm\rangle = \frac{|00\rangle \pm |11\rangle}{\sqrt{2}}$, and $|\Phi^\pm\rangle = \frac{|01\rangle \pm |10\rangle}{\sqrt{2}}$. It can be prepared employing Bell state measurements (BSM) that project two qubits onto one of the four maximally entangled Bell states, which has been efficiently realized in atomic [35] and optical platforms [36]. Imperfect Bell states such as the above could be the result of preparation in a non-ideal BSM setup.

The non-Hermitian Hamiltonian ($H_{\text{nh}}^{\text{Bell}}$) is constructed by choosing the imperfect Bell states as the set of right eigenvectors. Subsequently, the set of left eigenvectors can be obtained from the inverse of a matrix whose columns are the vectors $\{|R_m\rangle\}$. The unnormalized left eigenvectors are

$$\begin{aligned} |L_{1,2}\rangle &= \frac{\sqrt{1 + \alpha^2}}{2}(|00\rangle + (\alpha - 1)|01\rangle \pm \frac{1}{\alpha}|11\rangle), \\ |L_{3,4}\rangle &= \frac{\sqrt{(1 - \alpha)^2 + 2}}{2}(|01\rangle \pm |10\rangle). \end{aligned} \quad (17)$$

One can easily verify that the above vectors form a biorthonormal basis satisfying the relation

$$\langle L_m | R_n \rangle = \delta_{mn}, \quad \langle R_m | R_m \rangle = 1. \quad (18)$$

We now construct a non-Hermitian Hamiltonian using the basis states described in Eqs. (16) and (17) as

$$H_{\text{nh}}^{\text{Bell}} = \sum_m \lambda_m |R_m\rangle \langle L_m|, \quad (19)$$

where we choose the λ_m as real numbers [37], sampled from independent Gaussian distributions with zero

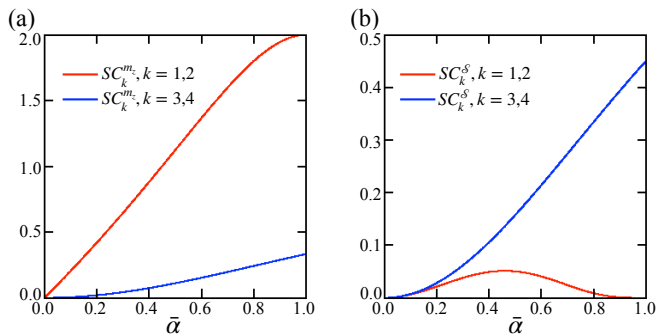


Figure 2. Non-Hermiticity at the level of single- and two-site quantum properties of the model constructed using imperfect Bell states. (a) Non-Hermiticity score $SC_k^{m_z}$ of a single-site quantum property, the z -magnetization, computed for both right as well as left eigenvectors. The maximum and the minimum ($SC_k^{m_z}$) values of the score are obtained for $k \in 1, 2$ and $k \in 3, 4$, respectively. In both cases, the behavior remains qualitatively the same as the Hamiltonian non-Hermiticity shown in Fig. 1(a). (b) Entanglement score, SC_k^S , obtained for the von Neumann entropy. Interestingly, the behavior obtained for quantum entanglement differs from the single-site score. In particular, unlike $SC_k^{m_z}$, SC_k^S attains its minimum value for $k = 1, 2$ and becomes maximum for $k = 3, 4$. Moreover, though $SC_{k=3,4}^S$ shows monotonic growth similar to $SC_k^{m_z}$ and $\mathcal{D}_{\min, \max}$, $SC_{k=1,2}^S$ vanishes for low as well as high values of $\bar{\alpha}$ and attains a maximum around $\bar{\alpha} = 0.449$.

mean and unit variance [38]. In recent years, such a bottom-up approach of reverse engineering a non-Hermitian quantum Hamiltonian from easily constructed eigenvectors got much attention in the community [39]. Below, we present the results obtained for both static and dynamical quantum properties related to the above non-Hermitian Hamiltonian.

1. Non-Hermiticity at the level of Hamiltonian: behavior of \mathcal{D} with α

We first examine how the degree of non-Hermiticity \mathcal{D} behaves for the Hamiltonian described in Eq. (19). For a fixed value of the parameter α , we compute \mathcal{D} for 1000 random realizations of H_{nh} by choosing its eigenvalues $\{\lambda_m\}$ from a Gaussian distribution with zero mean and unit variance. In Fig. 1(a), we plot the maximum as well as minimum among all the random realizations, denoted by \mathcal{D}_{\max} and \mathcal{D}_{\min} , respectively, against $\bar{\alpha} = 1 - \alpha$. At $\alpha = 1$ ($\bar{\alpha} = 0$), the right and left eigenvectors recover perfect Bell states and the Hamiltonian becomes Hermitian, reflected in vanishing \mathcal{D} . Though fluctuating, \mathcal{D}_{\min} tends to increase with $\bar{\alpha}$. The growth of \mathcal{D}_{\max} is smoother and at a faster rate, reaching the maximum non-Hermiticity of $\mathcal{D} = 1$ at $\bar{\alpha} = 1$.

2. Non-Hermiticity score for single-site property: magnetization

One of the main goals of our work is to examine to what extent the non-Hermiticity of the model Hamiltonian gets translated to its physical properties. Towards that aim, we now analyze the non-Hermiticity score for the magnetization in individual eigenstates. Results for quantum entanglement in individual eigenstates are presented in the following section. Analytical forms of all the quantities discussed in these two sections are provided in Appendix A. Two subsequent sections contain results for purity and entanglement under time evolution.

In Fig. 2(a), we plot the non-Hermiticity score for the magnetization of the first qubit (labeled A) along the z -axis, $\mathcal{F}[\rho] = m_z[\rho] = \text{Tr}(\hat{\sigma}_A^z \rho)$, $SC_k^{m_z} = |m_z[\rho_{RR}^k] - m_z[\rho_{LL}^k]|$. Here, $\hat{\sigma}^z$ is the 2×2 Pauli matrix along the z -direction and $\rho_{RR}^k = \frac{|R_k\rangle\langle R_k|}{\langle R_k|R_k\rangle}$, $\rho_{LL}^k = \frac{|L_k\rangle\langle L_k|}{\langle L_k|L_k\rangle}$, where $|R_k\rangle$ and $|L_k\rangle$ are individual right and left eigenvectors of $H_{\text{nh}}^{\text{Bell}}$, as given in Eqs. (16) and (17). As we are considering here properties of single eigenvectors, the eigenvalues λ_k do not directly enter the non-Hermiticity score, in contrast to \mathcal{D} discussed above, and no sampling over λ_k is necessary. To give an operational interpretation of the above observables, we may want to assume the eigenvalues to fulfill case 2 in Sec. II B, such that ρ_{RR}^k and ρ_{LL}^k are prepared when evolving an initial state to long times under $H_{\text{nh}}^{\text{Bell}}$ and $(H_{\text{nh}}^{\text{Bell}})^\dagger$, respectively.

As Fig. 2(a) shows, at each value of $\bar{\alpha}$, $SC_k^{m_z}$ achieves its maximum (minimum) for $k \in 1, 2$ ($3, 4$). Both the minimum and maximum of $SC_k^{m_z}$ increase monotonically with $\bar{\alpha}$ and agree qualitatively with \mathcal{D} as shown in Fig. 1(a). Moreover, $SC_{k=1,2}^{m_z}$ attains its theoretical maximum at $\bar{\alpha} = 1$. In other words, this single-particle property can serve as a probe of the non-Hermiticity of the model. Notably, for all values of α and any eigenvector k , m_z remains zero when computed for $\rho_{RL}^k = |R_k\rangle\langle L_k|$. Hence, the single-site quantum property obtained in the biorthogonal basis fails to capture any signature of the non-Hermiticity of the model.

3. Non-Hermiticity score for the von Neumann entropy (static case)

In this section, we analyze entanglement properties of the same set of right and left eigenvectors as considered above, in particular of the von Neumann entropy (VNE), defined as $\mathcal{S}[\rho] = -\text{Tr}_A(\text{Tr}_B(\rho) \log_2 \text{Tr}_B(\rho))$. Figure 2(b) presents the associated non-Hermiticity score, $SC_k^S = |\mathcal{S}[\rho_{RR}^k] - \mathcal{S}[\rho_{LL}^k]|$. Unlike the case for m_z , at each value of $\bar{\alpha}$, SC_k^S becomes minimum for $k = 1, 2$, and the behavior does not comply with \mathcal{D} . In particular, $SC_{k=1,2}^S$ vanishes both for $\bar{\alpha} \rightarrow 0$ and $\bar{\alpha} \rightarrow 1$, and attains a maximum around $\bar{\alpha} = 0.449$. This is significantly different from the behavior of \mathcal{D}_{\max} (or \mathcal{D}_{\min}) as well as the single-site property discussed above.

In contrast, the maximum value of $SC_k^{\mathcal{S}}$, attained for all values of $\bar{\alpha}$ at $k = 3, 4$, remains akin to \mathcal{D} . Nevertheless, quantitative differences remain. E.g., unlike \mathcal{D} , $SC_{k=3,4}^{\mathcal{S}}$ increases almost linearly in the region $0.4 \lesssim \bar{\alpha} \leq 1.0$ and goes to zero at $\bar{\alpha} = 0$. Moreover, $SC_{k=3,4}^{\mathcal{S}}$ does not reach its theoretical maximum of 1 at $\bar{\alpha} = 1$. Again, the VNE obtained for the biorthogonal ensemble $\rho_{RL}^k = |R_k\rangle\langle L_k|$ remains independent of $\bar{\alpha}$ (yielding the value $\mathcal{S}(|R_k\rangle\langle L_k|) = \frac{1}{2} \forall k$) and is thus not a useful probe for the non-Hermiticity of the system.

4. Non-Hermiticity score of global purity

In this section, we study the time-dependent non-Hermiticity score of the purity, $\mathcal{P}[\rho(t)] = \text{Tr}(\rho(t)^2) / \text{Tr}(\rho(t))^2$, of a state $\rho(t)$ obtained from an initial state ρ_{in} when evolved under $H_{\text{nh}}^{\text{Bell}}$ or $(H_{\text{nh}}^{\text{Bell}})^\dagger$. If the initial state is chosen as maximally mixed, $\rho_{\text{in}} = \frac{\mathbb{I}}{4}$, one gets $\mathcal{P}(\rho_{RR}(t)) = \mathcal{P}(\rho_{LL}(t))$ (see Appendix B). Hence, $SC^{\mathcal{P}}(t) = 0$ at all times and fails to witness any imprint of \mathcal{D} . However, for a non-maximally mixed initial state, $SC^{\mathcal{P}}(t)$ acquires a non-zero value. In Fig. 3, we plot the time-dependent purity score for systems initialized in a mixed Werner state, $\rho_W = \delta|\Psi^-\rangle\langle\Psi^-| + (1-\delta)\frac{\mathbb{I}}{4}$, with $|\Psi^-\rangle = \frac{|01\rangle - |10\rangle}{\sqrt{2}}$. We tune the initial purity to (a) $\delta = 0.1$, (b) $\delta = 0.5$, and (c) $\delta = 0.9$, and choose four different values of α , $\alpha = 0.1, 0.3, 0.6, 0.9$, which are depicted using lighter to darker shades of blue. In these plots, we fix the Hamiltonian eigenvalues to $\lambda_1 = 0.1$, $\lambda_2 = 0.2$, $\lambda_3 = 0.3$, and $\lambda_4 = 0.4$.

For all values of α and δ , $SC^{\mathcal{P}}(t)$ exhibits non-monotonic, periodic behavior with time. Moreover, at low δ , the highest value of the non-Hermiticity score within the considered time window, $SC_{\text{max}}^{\mathcal{P}} = \max_{t \in [0, 100]} \{SC^{\mathcal{P}}(t)\}$, depends on the parameter α . For instance, both at low and high values of α , $SC_{\text{max}}^{\mathcal{P}}$ remains low while it attains larger values at intermediate α . However, for initial states with higher purity, i.e., with larger δ [exemplified for $\delta = 0.9$ in Fig. 3(c)] $SC_{\text{max}}^{\mathcal{P}}$ decreases with increasing α . All these observations suggest \mathcal{P} does not imitate the profile of \mathcal{D} , and thus gives an independent imprint of non-Hermiticity on the time evolution.

5. Non-Hermiticity score of von Neumann entropy (dynamic case)

Further above, we have discussed the non-Hermiticity score for the VNE when computed for the special cases of $\rho_{RR}(t) \xrightarrow{t \rightarrow \infty} \rho_{RR}^k = |R_k\rangle\langle R_k|$ and $\rho_{LL}(t) \xrightarrow{t \rightarrow \infty} \rho_{LL}^k = |L_k\rangle\langle L_k|$. In this section, we consider a more general scenario where $\rho_{RR}(t)$ is obtained following Eq. (7) (and mutatis mutandis for $\rho_{LL}(t)$). Note that, in this case, the VNE is not an entanglement measure, as the global

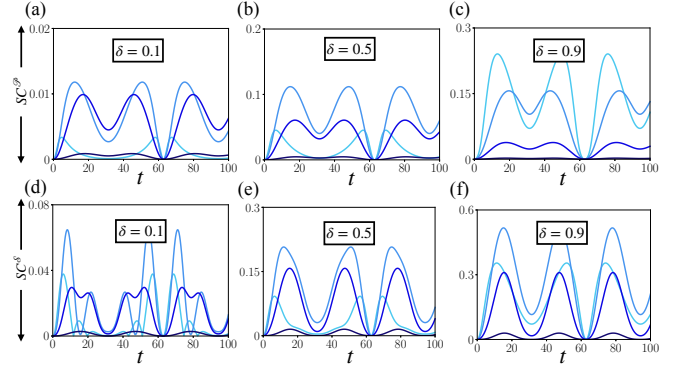


Figure 3. Behavior of non-Hermiticity score with time, for global purity \mathcal{P} and von Neumann entropy \mathcal{S} , computed for an initial state $\rho_W = \delta|\Psi^-\rangle\langle\Psi^-| + (1-\delta)\frac{\mathbb{I}}{4}$ subjected to evolution under $H_{\text{nh}}^{\text{Bell}}$ and $(H_{\text{nh}}^{\text{Bell}})^\dagger$. We probe the cases for $\alpha = 0.1, 0.3, 0.6, 0.9$ as shown using curves with darker to lighter shades of blue, and in all cases fix the Hamiltonian eigenvalues to $\lambda_1 = 0.1$, $\lambda_2 = 0.2$, $\lambda_3 = 0.3$, $\lambda_4 = 0.4$. (a)-(c) Purity score, $SC^{\mathcal{P}}(t)$ for (a) $\delta = 0.1$, (b) $\delta = 0.5$, and (c) $\delta = 0.9$. For large δ , the amplitude of $SC^{\mathcal{P}}(t)$ decreases with increasing α , while for small δ it attains a maximum at intermediate values of α . (d)-(f) Non-Hermiticity score for the VNE, $SC^{\mathcal{S}}(t)$, for same choices of δ .

states $\rho_{RR}(t)$ and $\rho_{LL}(t)$ are not pure. In Fig. 3(d)-(f), we plot the time-dependent behavior of $SC^{\mathcal{S}}(t) = |\mathcal{S}[\rho_{RR}(t)] - \mathcal{S}[\rho_{LL}(t)]|$, for the same parameter values as in panels (a)-(c). Similar to the purity score, $SC^{\mathcal{S}}$ exhibits non-monotonic behavior with time and its maximum value computed for the considered time period, $SC_{\text{max}}^{\mathcal{S}} = \max_{t \in [0, 100]} \{SC^{\mathcal{S}}(t)\}$, again remains low for high values of α . However, this score achieves significant values at small α even at large δ .

As these examples show, the non-Hermiticity score for dynamical physical quantities does not necessarily follow the profile of \mathcal{D} . In particular, $SC^{\mathcal{F}}$ can attain a low value even when the model Hamiltonian is highly non-Hermitian (in this case $\alpha \rightarrow 0$). One must thus distinguish between the non-Hermiticity of the model Hamiltonian and its imprint onto physical properties.

B. Non-Hermitian interacting Hatano–Nelson model

The second example system we consider is an interacting quantum many-body Hamiltonian, the non-Hermitian Hatano–Nelson model [40–43], defined by

$$H_{\text{nh}}^{\text{HN}} = \sum_i^N -J(e^{\chi}c_i^\dagger c_{i+1} + e^{-\chi}c_{i+1}^\dagger c_i) + V\hat{n}_i\hat{n}_{i+1}. \quad (20)$$

Here, the hopping strength $J = 1$ scales the Hamiltonian, $c_i^\dagger(c_i)$ is the creation (annihilation) operator for a spinless fermionic particle at site i , $\hat{n}_i = c_i^\dagger c_i$ the single-mode number operator, and V is the strength of nearest-

neighbor interaction. Moreover, we restrict our studies to the half-filling sector and employ periodic (anti-periodic) boundary conditions for odd (even) $N/2$. The notion of non-Hermiticity is introduced by asymmetric hopping controlled by the parameter χ , where the model reduces to the Hermitian version at $\chi = 0$. The model has parity-time (PT) reversal symmetry, which results in eigen energies appearing as complex conjugate pairs. In Ref. [43], it is reported that as the strength of the interaction (V) increases, the model undergoes two PT symmetry-breaking transitions: One of them is due to an exceptional point between the two lowest excited states and marked by the non-analytic behavior of the finite-size level-spacing $\Delta_{01} := \text{Re}(\lambda_1 - \lambda_0)$. The other corresponds to a full collapse of the complex many-body spectrum onto the real axis in a finite-size system. The former transition is accompanied by a first-order symmetry-breaking transition from a PT broken gapless phase to a PT-symmetric charge-density phase. Similar characteristics are also reported in the hardcore bosonic version of the model with periodic boundary condition [44]. In what follows, we present the results for the degree of Hamiltonian non-Hermiticity of the model as well as single- and multi-site non-Hermiticity scores, and also contrast their trend against the above-mentioned transitions.

1. *Hamiltonian non-Hermiticity (\mathcal{D}) in the interplay of asymmetric coupling (χ) and interactions (V)*

To begin with, we examine how the asymmetric coupling parameterized by χ and interaction strength V affect the degree of non-Hermiticity (\mathcal{D}) of the Hamiltonian $H_{\text{nh}}^{\text{HN}}$, plotted in Fig. 1(b). At $V = 0$, \mathcal{D} grows monotonously with χ and eventually saturates to the theoretical maximum of $\mathcal{D} \approx 2$. However, turning on even a small amount of interaction has a detrimental effect on \mathcal{D} : it attains a significant non-zero value only beyond a non-vanishing threshold coupling, χ_c . Interestingly, we further observe that up to $V \approx 10^3$, χ_c increases almost linearly with V . At even larger interaction strengths, \mathcal{D} remains zero up to the largest values of χ considered in our analysis ($\chi = 5.4$).

As these results show, interactions suppress the non-Hermiticity of the model significantly, as the distance between $H_{\text{nh}}^{\text{HN}}$ and $(H_{\text{nh}}^{\text{HN}})^\dagger$ becomes insignificant in comparison to the norm of $H_{\text{nh}}^{\text{HN}}$. Interestingly, the domain of vanishing \mathcal{D} coincides with the region of non-analyticity of Δ_{01} , which can be read off from Fig. 1(b) and its inset. This indicates that \mathcal{D} can be useful in detecting the PT symmetry-breaking transition present in the model. In turn, this may signify the importance of the normalization of \mathcal{D} considered in Eq. (13). In fact, the unnormalized incarnation of \mathcal{D} does not reveal any transition (see Appendix C). In the following, we will examine to what extent such a behavior reflects in the behavior of single- and multi-site quantum properties related to the model.

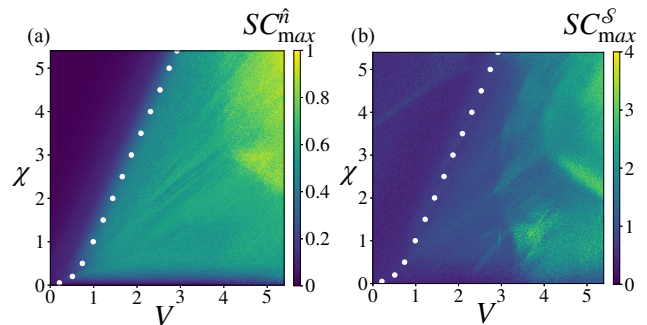


Figure 4. Comparison of non-Hermiticity at the level of the Hamiltonian and single- and multi-party physical properties of the non-Hermitian Hatano–Nelson model ($H_{\text{nh}}^{\text{HN}}$). We compute the non-Hermiticity score for both the number operator \hat{n} and half-chain VNE S for all the right and left eigenvectors of the model and finally compute the maximum among all of them. (a) Depicts the behavior of $SC_{\max}^{\hat{n}}$ in the $V - \chi$ plane. We note that for a large region in the parameter space, the behavior of $SC_{\max}^{\hat{n}}$ remains almost complementary to \mathcal{D} , as shown in Fig. 1(b). A similar plot for the half-chain VNE is presented in (b), where for the same set of parameters, we plot the behavior of SC_{\max}^S . We note that SC_{\max}^S behaves differently from both $SC_{\max}^{\hat{n}}$ as well as the degree of non-Hermiticity (\mathcal{D}). In particular, SC_{\max}^S attains significant value only when both V and χ take large values. However, closer inspection shows the qualitative agreement between the trend of $SC_{\max}^{\hat{n}}$ and SC_{\max}^S . The white circles correspond to the PT symmetry-breaking transition marked by the non-analytic behavior of Δ_{01} defined in Sec. III B and shown in the inset of Fig. 1. We notice the agreement between the PT symmetry-breaking transition and domain for vanishing scores. The data is reported for $N = 12$ sites, half-filling, and with anti-periodic boundary conditions.

2. *Single-site properties: non-Hermiticity score of number operator \hat{n}*

To study the impact of non-Hermiticity on single-site properties, we analyze the non-Hermiticity score of the number operator for the first site, \hat{n}_1 . The maximum score over all eigenstates, $SC_{\max}^{\hat{n}} \equiv \|SC_{\text{nh}}^{\hat{n}}\|_{\infty}$, is plotted in Fig. 4(a). Importantly, $SC_{\max}^{\hat{n}}$ exhibits an almost complementary behavior to the non-Hermiticity of the Hamiltonian \mathcal{D} . In particular, at low values of interaction, $SC_{\max}^{\hat{n}}$ becomes almost zero. Once the strength of the interaction is increased, expectation values of the single-site occupation evaluated in right and left eigenvectors start to exhibit a disparity, which is captured by significantly non-zero values of $SC_{\max}^{\hat{n}}$ within an intermediate regime of χ . Throughout the entire window of interaction strengths considered, $SC_{\max}^{\hat{n}}$ vanishes at small χ , while beyond $V \approx 10^2$ the non-vanishing region extends up to the maximum value of χ that we have considered. The region of V where $SC_{\max}^{\hat{n}}$ becomes finite for any χ resides in close proximity to the PT symmetry-breaking transition marked by the non-analytic point of Δ_{01} . Thereby,

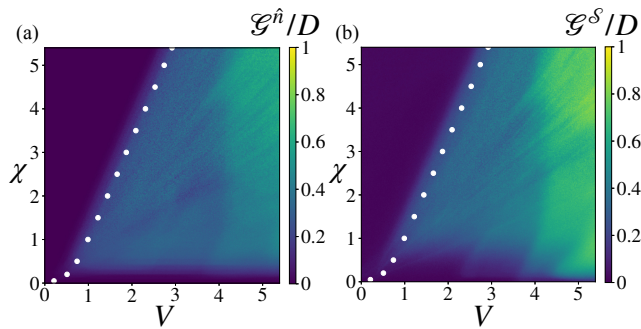


Figure 5. Global characteristics of $\overline{SC_{\text{nh}}^{\mathcal{F}}}$ for the non-Hermitian Hatano–Nelson model ($H_{\text{nh}}^{\text{HN}}$). We compute the total number of elements of $SC_{\text{nh}}^{\hat{n}}$ and $SC_{\text{nh}}^{\mathcal{S}}$ with the conditions $SC_{\text{nh}}^{\hat{n}}[k] \geq \mathcal{E}_{\text{Th}}^{\hat{n}}$ and $SC_{\text{nh}}^{\mathcal{S}}[k] \geq \mathcal{E}_{\text{Th}}^{\mathcal{S}}$, respectively, where $k = 1, 2, \dots, D$ with D being the Hilbert space dimension. These quantities, scaled by D , are shown in (a) and (b). We obtain a similar trend as in Fig. 4. Data for threshold values $\mathcal{E}_{\text{Th}}^{\hat{n}} = \mathcal{E}_{\text{Th}}^{\mathcal{S}} = 0.1$. Similar to Figs. 1 and 4, the white circles correspond to the PT symmetry-breaking transition. The data is reported for $N = 12$ sites, half-filling, and with anti-periodic boundary conditions.

$SC_{\text{max}}^{\hat{n}}$ can be considered as another candidate in identifying the PT symmetry-breaking transition of the model.

In summary, the complementary behavior of $SC_{\text{max}}^{\hat{n}}$ to \mathcal{D} suggests that the single-particle quantum property of the model can be a useful probe in detecting the non-Hermiticity of the model.

Unlike the case of $H_{\text{nh}}^{\text{Bell}}$, here the spectrum of the Hamiltonian consists of a large number of eigenvectors. Therefore, to illustrate the non-Hermitian behavior across the spectrum of the model, in Fig. 5(a) we plot the quantity $\mathcal{G}^{\hat{n}}$, see Sec. II C 2, choosing as threshold value $\mathcal{E}_{\text{Th}}^{\hat{n}} = 0.1$. The behavior is qualitatively similar to the one of $SC_{\text{max}}^{\hat{n}}$, showing that in this case, the maximal score is representative of the behavior across the spectrum.

3. Multi-site properties: non-Hermiticity score of von Neumann entropy

As a multipartite quantum property, here we analyze the non-Hermiticity score computed for half-chain VNE, defined as $SC^{\mathcal{S}} = |\mathcal{S}[\rho_{RR}] - \mathcal{S}[\rho_{LL}]|$, where $\rho_{RR} = \text{Tr}_{N/2+1 \dots N}(|R_k\rangle\langle R_k|)$ and $\rho_{LL} = \text{Tr}_{N/2+1 \dots N}(|L_k\rangle\langle L_k|)$, with $|R_k\rangle$ and $\langle L_k|$ the k -th right and left vectors of $H_{\text{nh}}^{\text{HN}}$, respectively. In Fig. 4(b), we plot the maximum of $SC^{\mathcal{S}}$ over all the eigenstates of the model, $SC_{\text{max}}^{\mathcal{S}}$.

In this case, the behavior of $SC_{\text{max}}^{\mathcal{S}}$ remains qualitatively similar to $SC_{\text{max}}^{\hat{n}}$. In particular, $SC_{\text{max}}^{\mathcal{S}}$ starts attaining significant nonzero value after a threshold value of the interaction strength that exhibits almost linear behavior with the coupling χ . Moreover, similar to the single-particle case, in most of the considered regimes,

multipartite quantum properties of the right and left ensembles remain very much distinguishable from each other. Such a disparity becomes maximum when both interaction and the coupling become very large.

Furthermore, we report that $\mathcal{G}^{\mathcal{S}}$, i.e., the number of eigenstates with $SC^{\mathcal{S}}$ above a threshold that we choose as $\mathcal{E}_{\text{Th}}^{\mathcal{S}} = 0.1$, shows behavior similar to the $\mathcal{G}^{\hat{n}}$ as well as $SC_{\text{max}}^{\mathcal{S}}$. Similar to the previous cases, the PT symmetry-breaking transition region qualitatively coincides to the domain where $\mathcal{G}^{\mathcal{S}}$ becomes finite.

IV. DISCUSSION

In this work, we have introduced a formalism that quantifies different notions of non-Hermiticity, which can emerge in any generic non-Hermitian system. In particular, as first quantifier, we have introduced the Hamiltonian non-Hermiticity, a measure that computes the normalized distance between a non-Hermitian Hamiltonian H_{nh} and its hermitian conjugate $(H_{\text{nh}})^{\dagger}$. We have introduced a second quantifier to capture a notion of non-Hermiticity at the level of physically computable quantities related to the model. This quantifier has been motivated by noticing that in the non-Hermitian paradigm one can prepare quantum ensembles of right or left eigenvectors, which often yield incompatible results with respect to single- and multi-site quantum properties. Based on this observation, we have introduced the non-Hermiticity score that characterized the difference between observables in the right and left eigenensemble. These quantifiers enable a comparative study of the degree of non-Hermiticity across different regions of parameter space, for static as well as dynamic properties.

We have tested the formalism on two examples, in their static eigenstates as well as time evolution. The first non-Hermitian model we have considered has quantum information-theoretic origin, namely a non-Hermitian Hamiltonian constructed using a set of imperfect Bell states. We showed that though the qualitative behavior of the non-Hermiticity score computed for a single-site observable complies with the degree of non-Hermiticity of the model, in the case of the von Neumann entropy their behavior significantly differs.

Second, we have applied our formalism to a more generic case, to a quantum many-body model in the form of the interacting Hatano–Nelson model with asymmetric coupling. The model gives us a scope to examine how both interaction and hopping affect the behavior of distinct notions of non-Hermiticity. For the Hamiltonian non-Hermiticity, interaction has an adverse effect. Importantly, for the non-Hermiticity score of single- and multi-site quantum properties, the behavior is more involved. For instance, the non-Hermiticity score of the single-site number operator \hat{n} remains almost complementary to the behavior of the degree of non-Hermiticity of the Hamiltonian. This implies that even at large interactions, when the non-Hermitian part of the Hamiltonian

gets strongly suppressed, locally the left and right vectors can be significantly different from each other. Finally, we have examined to what extent the non-Hermiticity of the model gets translated into the behavior of entanglement. At first glance it appears that the behavior of non-Hermiticity does not vary smoothly with both interaction strength and coupling. However, a careful look reveals that for a significant region of the considered parameter range, in relation to entanglement the left and right ensembles behave distinctly from each other and the difference qualitatively mimics the behavior obtained for the single-particle case. Furthermore, we obtain qualitative agreement between the PT symmetry-breaking transition regime of the model with the domain where the scores become zero to finite or vice-versa. This indicates that the non-Hermitian scores can be useful in identifying potential non-Hermitian phase transitions in a model.

In summary, in our work we have opened a new route to examining the quantum properties of any generic non-Hermitian system. It permits to quantify non-Hermiticity, not only along the traditional lines that solely focuses on the Hamiltonian of the model but also in respect to its influence onto observable properties. We believe our formalism can be instrumental in characterizing exotic quantum many-body phases, identifying potential non-Hermitian phase transitions, as well as in the preparation of resourceful quantum states for quantum technologies. As an application of this proposed framework, in future work we aim to apply it to gain a deeper understanding of non-Hermitian topological systems.

ACKNOWLEDGMENTS

This project is funded by the European Union under NextGenerationEU. PRIN 2022 Prot. n. 2022ATM8FY (CUP: E53D23002240006). This project has received funding from the Italian Ministry of University and Research (MUR) through the FARE grant for the project DAVNE (Grant R20PEX7Y3A). The project is funded under the National Recovery and Resilience Plan (NRRP), Mission 4 Component 2 Investment 1.4 - Call for tender No. 1031 of 17/06/2022 of Italian Ministry for University and Research funded by the European Union – NextGenerationEU (proj. nr. CN_00000013). This work was supported by the Swiss State Secretariat for Education, Research and innovation (SERI) under contract number UeMO19-5.1. Project DYNAMITE QUANTERA2_00056 funded by the Ministry of University and Research through the ERANET COFUND QuantERA II – 2021 call and co-funded by the European Union (H2020, GA No 101017733). Views and opinions expressed are however those of the author(s) only and do not necessarily reflect those of the European Union or of the Ministry of University and Research. Neither the European Union nor the granting authority can be held responsible for them. This work was supported by the Provincia Autonoma di Trento, and Q@TN, the joint lab between University of Trento, FBK—Fondazione Bruno Kessler, INFN—National Institute for Nuclear Physics, and CNR—National Research Council. S.B. acknowledges CINECA for the use of HPC resources under IS CRA-C project DISYK (HP10CGNZG9).

Appendix A: Derivation of analytical of magnetization and entanglement for imperfect Bell states

In this appendix, we present the analytical form of the magnetization and quantum entanglement computed for the set of left and right eigenvectors of the non-Hermitian Hamiltonian $H_{\text{nh}}^{\text{Bell}}$. Values of m_z evaluated for the ensembles of right and left eigenvectors of $H_{\text{nh}}^{\text{Bell}}$ are given in the following table:

Index (m)	$m_z = \text{Tr}(\hat{\sigma}_z \rho_m^L), \rho_m^L = \text{Tr}_1[L_m\rangle\langle L_m]$	$m_z = \text{Tr}(\hat{\sigma}_z \rho_m^R), \rho_m^R = \text{Tr}_1[R_m\rangle\langle R_m]$
1	$\frac{\alpha^2 + \alpha^2(\alpha-1)^2 - 1}{\alpha^2 + \alpha^2(\alpha-1)^2 + 1}$	$\frac{1 - \alpha^2}{1 + \alpha^2}$
2	$\frac{\alpha^2 + \alpha^2(\alpha-1)^2 - 1}{\alpha^2 + \alpha^2(\alpha-1)^2 + 1}$	$\frac{1 - \alpha^2}{1 + \alpha^2}$
3	0	$\frac{(1 - \alpha)^2}{2 + (1 - \alpha)^2}$
4	0	$\frac{(1 - \alpha)^2}{2 + (1 - \alpha)^2}$

We can write the entanglement entropy as $\mathcal{S}(|R_m\rangle\langle R_m|) = -\lambda_m^R \log(\lambda_m^R) - (1 - \lambda_m^R) \log(1 - \lambda_m^R)$ and $\mathcal{S}(|L_m\rangle\langle L_m|) = -\lambda_m^L \log(\lambda_m^L) - (1 - \lambda_m^L) \log(1 - \lambda_m^L)$. Analytical forms of the quantities λ_m^R and λ_m^L are:

Index (m)	λ_m^L	λ_m^R
1	$\frac{1}{2} + \frac{\sqrt{1 - \frac{4\alpha^2}{(\alpha^2 + \alpha^2(\alpha-1)^2 + 1)^2}}}{2}$	$\frac{1}{1+\alpha^2}$
2	$\frac{1}{2} + \frac{\sqrt{1 - \frac{4\alpha^2}{(\alpha^2 + \alpha^2(\alpha-1)^2 + 1)^2}}}{2}$	$\frac{1}{1+\alpha^2}$
3	$\frac{1}{2}$	$\frac{1}{2} + \frac{\sqrt{1 - \frac{4}{(2+(\alpha-1)^2)^2}}}{2}$
4	$\frac{1}{2}$	$\frac{1}{2} + \frac{\sqrt{1 - \frac{4}{(2+(\alpha-1)^2)^2}}}{2}$

Appendix B: Purity score for maximally mixed input state

In this section, we give the analytical derivation for the purity score of the model given by imperfect Bell states. The purity of the ensemble evolved under $H_{\text{nh}}^{\text{Bell}}$ is

$$\mathcal{P}(\rho_{RR}(t)) = \frac{\text{Tr}[\rho_{RR}(t)^2]}{\text{Tr}(\rho_{RR}(t))^2} = \frac{\sum_{mnm'n'} p_{mn} p_{m'n'} \langle R_{n'} | R_m \rangle \langle R_n | R_{m'} \rangle}{\left(\sum_{mn} p_{mn} \langle R_n | R_m \rangle \right)^2}, \quad (\text{B1})$$

with $p_{mn} = e^{-i(\lambda_m - \lambda_n)t} \langle L_m | \rho_{\text{in}} | L_n \rangle$. Similarly, for the quantum state evolved under $(H_{\text{nh}}^{\text{Bell}})^\dagger$, we get

$$\mathcal{P}(\rho_{LL}(t)) = \frac{\text{Tr}[\rho_{LL}(t)^2]}{\text{Tr}(\rho_{LL}(t))^2} = \frac{\sum_{mn,m'n'} \tilde{p}_{mn} \tilde{p}_{m'n'} \langle L_{n'} | L_m \rangle \langle L_n | L_{m'} \rangle}{\left(\sum_{mn} \tilde{p}_{mn} \langle L_n | L_m \rangle \right)^2}, \quad (\text{B2})$$

with $\tilde{p}_{mn} = e^{-i(\lambda_m - \lambda_n)t} \langle R_m | \rho_{\text{in}} | R_n \rangle$.

Now, for a maximally mixed initial state $\rho = \frac{\mathbb{1}}{4}$, from Eq. (B1) we get

$$\begin{aligned} \mathcal{P}(\rho_{RR}(t)) &= \frac{\sum_{mnm'n'} \langle L_m | L_n \rangle \langle L_{m'} | L_{n'} \rangle \langle R_{n'} | R_m \rangle \langle R_n | R_{m'} \rangle}{\left(\sum_{mn} \langle L_m | L_n \rangle \langle R_n | R_m \rangle \right)^2} \\ &= \frac{\sum_{mnm'n'} \langle L_n | L_m \rangle \langle L_{n'} | L_{m'} \rangle \langle R_m | R_{n'} \rangle \langle R_{m'} | R_n \rangle}{\left(\sum_{mn} \langle L_n | L_m \rangle \langle R_m | R_n \rangle \right)^2} \quad (\text{taking the conjugate of all the overlaps}) \\ &= \frac{\sum_{mnm'n'} \langle R_m | R_n \rangle \langle R_{m'} | R_{n'} \rangle \langle L_{n'} | L_m \rangle \langle L_n | L_{m'} \rangle}{\left(\sum_{mn} \langle L_n | L_m \rangle \langle R_m | R_n \rangle \right)^2} \quad (\text{exchanging indices } n \text{ and } n') \\ &= \mathcal{P}(\rho_{LL}(t)). \end{aligned} \quad (\text{B3})$$

Hence, for a maximally mixed initial state, the purity obtained at any time remains exactly the same for the left and right ensembles and thus the non-Hermiticity score for the purity vanishes.

Appendix C: Behavior of $\tilde{\mathcal{D}} = |H_{\text{nh}}^{\text{HN}} - (H_{\text{nh}}^{\text{HN}})^\dagger|$ in the $V - \chi$ plane

In this appendix, we present numerical results using—rather than the normalized Hamiltonian non-Hermiticity score, Eq. (13)—the unnormalized norm $\tilde{\mathcal{D}} = |H_{\text{nh}}^{\text{HN}} - (H_{\text{nh}}^{\text{HN}})^\dagger|$. Figure 6 shows the results computed for the interacting Hatano–Nelson model. As may have been expected, the distance between $H_{\text{nh}}^{\text{HN}}$ and its Hermitian conjugate $(H_{\text{nh}}^{\text{HN}})^\dagger$ depends only on the strength of the asymmetric hopping χ . As a consequence, the use of the unnormalized form would suggest physics that remains completely independent of the interaction strength V . In particular, it does not capture in any way the changes that occur in the observable scores as V is increased [see Figs. 4 and 5 of the main text]. Moreover, at large interaction the non-Hermitian part becomes insignificant in comparison to the interactions. We thus find it more suitable to normalize by the operator norm $|H_{\text{nh}}^{\text{HN}}|$ to obtain a non-Hermitian score \mathcal{D} corresponding to a Hamiltonian with fixed bandwidth [as given in Eq. (13) and Fig. 1(b) of the main text].

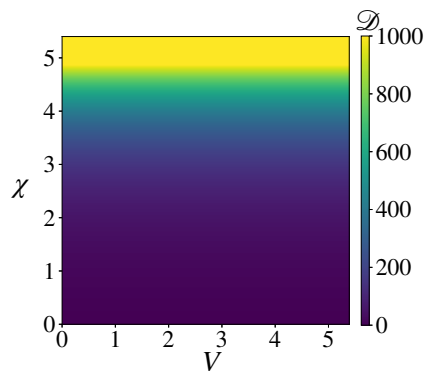


Figure 6. Unnormalized degree of non-Hermiticity $\tilde{\mathcal{D}} = \|H_{\text{nh}}^{\text{HN}} - (H_{\text{nh}}^{\text{HN}})^\dagger\|$ for the interacting non-Hermitian Hatano–Nelson model as in Fig. 1(b). The distance between $H_{\text{nh}}^{\text{HN}}$ and its Hermitian conjugate $(H_{\text{nh}}^{\text{HN}})^\dagger$ remains independent of the interaction term V and simply increases monotonically with the strength of the asymmetric hopping χ .

-
- [1] L. Feng, R. El-Ganainy, and L. Ge, Non-Hermitian photonics based on parity–time symmetry, *Nat. Photon.* **11**, 752 (2017).
- [2] M.-A. Miri and A. Alù, Exceptional points in optics and photonics, *Science* **363**, eaar7709 (2019).
- [3] Y. Ashida, Z. Gong, and M. Ueda, Non-Hermitian physics, *Advances in Physics* **69**, 249 (2020).
- [4] W. Chen, M. Abbasi, Y. N. Joglekar, and K. W. Murch, Quantum jumps in the non-Hermitian dynamics of a superconducting qubit, *Phys. Rev. Lett.* **127**, 140504 (2021).
- [5] S. Gopalakrishnan and M. J. Gullans, Entanglement and purification transitions in non-Hermitian quantum mechanics, *Phys. Rev. Lett.* **126**, 170503 (2021).
- [6] V. Meden, L. Grunwald, and D. M. Kennes, \mathcal{PT} -symmetric, non-Hermitian quantum many-body physics—a methodological perspective, *Rep. Prog. Phys.* **86**, 124501 (2023).
- [7] F. Minganti, A. Miranowicz, R. W. Chhajlany, and F. Nori, Quantum exceptional points of non-Hermitian Hamiltonians and Liouvillians: The effects of quantum jumps, *Phys. Rev. A* **100**, 062131 (2019).
- [8] L. Xiao, T. Deng, K. Wang, G. Zhu, Z. Wang, W. Yi, and P. Xue, Non-Hermitian bulk–boundary correspondence in quantum dynamics, *Nat. Phys.* **16**, 761 (2020).
- [9] A. Ghatak and T. Das, New topological invariants in non-Hermitian systems, *J. Phys.: Condens. Matter* **31**, 263001 (2019).
- [10] E. J. Bergholtz, J. C. Budich, and F. K. Kunst, Exceptional topology of non-Hermitian systems, *Rev. Mod. Phys.* **93**, 015005 (2021).
- [11] G. Cipolloni and J. Kudler-Flam, Non-Hermitian Hamiltonians violate the eigenstate thermalization hypothesis, *Phys. Rev. B* **109**, L020201 (2024).
- [12] S. S. Roy, S. Bandyopadhyay, R. C. de Almeida, and P. Hauke, Unveiling eigenstate thermalization for non-Hermitian systems, (2023), [arXiv:2309.00049 \[quant-ph\]](https://arxiv.org/abs/2309.00049).
- [13] R. Hamazaki, K. Kawabata, and M. Ueda, Non-Hermitian many-body localization, *Phys. Rev. Lett.* **123**, 090603 (2019).
- [14] S. Khandelwal, N. Brunner, and G. Haack, Signatures of liouvillian exceptional points in a quantum thermal machine, *PRX Quantum* **2**, 040346 (2021).
- [15] M. Am-Shallem, R. Kosloff, and N. Moiseyev, Exceptional points for parameter estimation in open quantum systems: analysis of the bloch equations, *New J. Phys.* **17**, 113036 (2015).
- [16] H. Hodaei, A. U. Hassan, S. Wittek, H. Garcia-Gracia, R. El-Ganainy, D. N. Christodoulides, and M. Khajavikhan, Enhanced sensitivity at higher-order exceptional points, *Nature* **548**, 187 (2017).
- [17] H.-K. Lau and A. A. Clerk, Fundamental limits and non-reciprocal approaches in non-Hermitian quantum sensing, *Nat. Commun.* **9**, 4320 (2018).
- [18] W. Chen, Ş. Kaya Özdemir, G. Zhao, J. Wiersig, and L. Yang, Exceptional points enhance sensing in an optical microcavity, *Nature* **548**, 192 (2017).
- [19] M. Naghiloo, M. Abbasi, Y. N. Joglekar, and K. W. Murch, Quantum state tomography across the exceptional point in a single dissipative qubit, *Nat. Phys.* **15**, 1232 (2019).
- [20] L. Herviou, N. Regnault, and J. H. Bardarson, Entanglement spectrum and symmetries in non-Hermitian fermionic non-interacting models, *SciPost Phys.* **7**, 069 (2019).
- [21] K. Kawabata, K. Shiozaki, and S. Ryu, Many-body topology of non-Hermitian systems, *Phys. Rev. B* **105**, 165137 (2022).
- [22] R. Modak and B. P. Mandal, Eigenstate entanglement entropy in a \mathcal{PT} -invariant non-Hermitian system, *Phys. Rev. A* **103**, 062416 (2021).
- [23] H. P. Breuer and F. Petruccione, *The Theory of Open Quantum Systems* (Oxford University Press, Great Clarendon Street, 2002).
- [24] C. M. Bender, D. C. Brody, H. F. Jones, and B. K. Meister, Faster than Hermitian quantum mechanics, *Phys. Rev. Lett.* **98**, 040403 (2007).
- [25] U. Günther and B. F. Samsonov, Naimark-dilated \mathcal{PT} -symmetric brachistochrone, *Phys. Rev. Lett.* **101**, 230404 (2008).
- [26] Y. Wu, W. Liu, J. Geng, X. Song, X. Ye, C.-K. Duan, X. Rong, and J. Du, Observation of parity-time symme-

- try breaking in a single-spin system, *Science* **364**, 878 (2019).
- [27] J. Wen, C. Zheng, X. Kong, S. Wei, T. Xin, and G. Long, Experimental demonstration of a digital quantum simulation of a general \mathcal{PT} -symmetric system, *Phys. Rev. A* **99**, 062122 (2019).
- [28] R. Grimaudo, A. Messina, A. Sergi, N. V. Vitanov, and S. N. Filippov, Two-qubit entanglement generation through non-Hermitian Hamiltonians induced by repeated measurements on an ancilla, *Entropy* **22**, 10.3390/e22101184 (2020).
- [29] H. Liu, X. Yang, K. Tang, L. Che, X. Nie, T. Xin, J. Li, and D. Lu, Practical quantum simulation of small-scale non-Hermitian dynamics, *Phys. Rev. A* **107**, 062608 (2023).
- [30] A. J. Daley, Quantum trajectories and open many-body quantum systems, *Advances in Physics* **63**, 77 (2014).
- [31] K. T. Geier and P. Hauke, From non-Hermitian linear response to dynamical correlations and fluctuation-dissipation relations in quantum many-body systems, *PRX Quantum* **3**, 030308 (2022).
- [32] K. Koshino and A. Shimizu, Quantum Zeno effect by general measurements, *Physics Reports* **412**, 191 (2005).
- [33] P. Facchi and S. Pascazio, Quantum Zeno dynamics: mathematical and physical aspects, *J. Phys. A: Math. Theor.* **41**, 493001 (2008).
- [34] A. McDonald, R. Hanai, and A. A. Clerk, Nonequilibrium stationary states of quantum non-Hermitian lattice models, *Phys. Rev. B* **105**, 064302 (2022).
- [35] N. Schine, A. W. Young, W. J. Eckner, M. J. Martin, and A. M. Kaufman, Long-lived bell states in an array of optical clock qubits, *Nat. Phys.* **18**, 1067 (2022).
- [36] C. K. Hong, Z. Y. Ou, and L. Mandel, Measurement of subpicosecond time intervals between two photons by interference, *Phys. Rev. Lett.* **59**, 2044 (1987).
- [37] C. M. Bender and S. Boettcher, Real spectra in non-Hermitian Hamiltonians having \mathcal{PT} symmetry, *Phys. Rev. Lett.* **80**, 5243 (1998).
- [38] We find that for other choices of the variance there is no significant change in the behavior of $\mathcal{D}_{\min(max)}$.
- [39] R. Shen, Y. Guo, and S. Yang, Construction of non-Hermitian parent Hamiltonian from matrix product states, *Phys. Rev. Lett.* **130**, 220401 (2023).
- [40] N. Hatano and D. R. Nelson, Localization transitions in non-Hermitian quantum mechanics, *Phys. Rev. Lett.* **77**, 570 (1996).
- [41] N. Hatano and D. R. Nelson, Vortex pinning and non-Hermitian quantum mechanics, *Phys. Rev. B* **56**, 8651 (1997).
- [42] N. Hatano and D. R. Nelson, Non-Hermitian delocalization and eigenfunctions, *Phys. Rev. B* **58**, 8384 (1998).
- [43] S.-B. Zhang, M. M. Denner, T. c. v. Bzdušek, M. A. Sentef, and T. Neupert, Symmetry breaking and spectral structure of the interacting Hatano-Nelson model, *Phys. Rev. B* **106**, L121102 (2022).
- [44] C.-Z. Lu and G. Sun, Many-body entanglement and spectral clusters in the extended hard-core bosonic Hatano-Nelson model, *Phys. Rev. A* **109**, 042208 (2024).